

Earth and Space Science

RESEARCH ARTICLE

10.1029/2020EA001336

Special Section:
InSight at Mars

Key Points:

- InSight color measurements agree with results from Viking, Mars Pathfinder, and the Mars Exploration Rovers
- Measured color properties are composed of two distinct color endpoints: rocky material that is spectrally flat, and yellowish-brown dust
- All observed colors at the landing site are mixtures of these two endpoint members, modified by Mars daylight
- Measurements of Martian daylight chromaticity show that the color that is slightly redder than Earth daylight (by $\delta x = 0.04$ and $\delta y = 0.01$)

Correspondence to:

J. N. Maki,
Justin.N.Maki@jpl.nasa.gov

Citation:

Maki, J. N., Golombek, M., Banerdt, W., Smrekar, S., Deen, R., Abarca, H., et al. (2021). Color properties at the Mars InSight landing site. *Earth and Space Science*, 8, e2020EA001336. <https://doi.org/10.1029/2020EA001336>

Received 16 OCT 2020
Accepted 1 DEC 2020

© 2020. Jet Propulsion Laboratory, California Institute of Technology. Government sponsorship acknowledged.

This is an open access article under the terms of the Creative Commons Attribution License, which permits use, distribution and reproduction in any medium, provided the original work is properly cited.

Color Properties at the Mars InSight Landing Site

J. N. Maki¹ , M. Golombek¹ , W. Banerdt¹, S. Smrekar¹ , R. Deen¹ , H. Abarca¹, S. Lu¹ , and J. Hall¹

¹Jet Propulsion Laboratory, California Institute of Technology, Pasadena, CA, USA



Abstract The color properties observed at the InSight landing site by the lander cameras are spectral mixtures of two source materials: gray-black rocky material with chromaticity values of $x = 0.32$, $y = 0.32$ (standard deviations of $\sigma_x = 0.02$ and $\sigma_y = 0.03$) and yellowish-brown dust with chromaticity values of $x = 0.42$, $y = 0.36$ (standard deviations of $\sigma_x = 0.02$ and $\sigma_y = 0.03$). These results are consistent with published values from other Mars landed missions. The InSight measurements also include the first published value of the white point of Mars daylight, chromaticity of $x = 0.35$, $y = 0.34$ (standard deviations of $\sigma_x = 0.01$ and $\sigma_y = 0.02$), which is redder than earth daylight by $\delta x = 0.04$ and $\delta y = 0.01$. InSight measurements also show a small color difference ($\delta x = 0.02$ and $\delta y = 0.01$) between the near field terrain (within 20 m of the lander) and the far field area beyond. This color difference is believed to be caused by dust being blown off by near field terrain by the lander rockets during the landing event. The visual difference between these two regions is caused primarily by the brightness variation. Chromaticity measurements of the Martian sky also match previous missions with additional variability caused by differences in dust loading and the dynamic nature of the Martian atmosphere.

Plain Language Summary Calibrated color images acquired at the InSight landing site show colors that fall into two broad categories, dark gray rocky material and yellowish-brown dust, consistent with previous Mars lander missions.

1. Introduction

The work described here demonstrates how three-channel visible color image data can be tied to a well-established colorimetric reference standard. This work uses data acquired at the Mars InSight landing site by the color cameras on the InSight lander (J. N. Maki et al., 2018). After landing on November 26, 2018 the lander began returning color images of the landing site (Figure 1). These images were primarily used to deploy a seismometer and heat flow probe onto the Martian surface using a robotic arm (Banerdt et al., 2020). The images were also used to assess of the geology at the landing site (Golombek et al., 2020).

1.1. Color Images

Image data returned from a landed Mars mission create the context from which the entire science and engineering teams conduct surface operations, and color is an important part of this context. While many people know that Mars is red, a calibrated color image tells us more specifically that Mars is a yellowish-brown color with a chromaticity coordinate of $x = 0.42$, $y = 0.36$, with standard deviations of $\sigma_x = 0.02$ and $\sigma_y = 0.03$. This type of quantitative analysis allows a comparison against other materials and images within a landing site, at different times of day, and across multiple landing sites. Color information also plays an important role in assessing the level of dustiness of a material in a way that is difficult to do with only a black/white image. As shown in this study, the color of a material is very dependent on the level of dustiness of the material. Rocks near the InSight lander that were cleared of dust by the InSight lander rockets provide a relatively dust-free colorimetric reference point to compare against.

1.2. Previous Work

Mars is named after the Roman god of war because of its reddish color, and other ancient civilizations named the planet with words that also describe a reddish color (IAU, 2020). Later spectroscopic observations



Figure 1. A calibrated color Instrument Deployment Camera (IDC) image, D000M0008_597250940CPG_F0000_0133M2, acquired on Sol 8 at a local true solar time of 15:27.

of Mars suggested that this reddish color is caused primarily by strong iron oxide (Fe^{3+}) absorption (Singer, 1982), but the detailed mineralogical story of Martian materials is still a work in progress (Ehlmann & Edwards, 2014).

Color cameras have returned detailed images from the surface of Mars, as described in Mutch et al. (1976), Smith et al. (1997b), Bell et al., (2003), and Malin et al. (2017). The first calibrated color measurements from a landed Mars mission are from Viking (Huck et al., 1977). Huck et al. showed that the color of Mars was a yellowish brown, with the chromaticity values for the soil ranging from ($x = 0.43$ to 0.46 , and $y = 0.39$ to 0.40), with the most common chromaticity value being ($x = 0.44$, $y = 0.40$). The second set of published color measurements came from J. N. Maki et al. (1999) using data acquired at the Mars Pathfinder landing site. The Pathfinder results matched Viking, with chromaticity measurements from both missions showing a range of soil chromaticity values from ($x = 0.43$ to 0.45) and ($y = 0.38$ to 0.41). Maki et al. also published the first chromaticity values for rocky material, with values ranging from ($x = 0.38$ to 0.41) and ($y = 0.35$ to 0.39), indicating that the rocky material, while darker, also exhibited a slightly bluer color. In 2006, Bell et al. published a set of Mars sky chromaticities from the Mars Exploration Rover (MER) missions, consistent with the previously published values from Huck et al. (1977) and J. N. Maki et al. (1999). Bell also published a single value for soil chromaticity ($x = 0.434$ and $y = 0.394$), also consistent with Viking and Mars Pathfinder. All of these results consistently showed the colors of the landing site were derived from dark gray basaltic materials and bright yellowish brown dust material. Most of the colors at the landing sites were mixtures of these two materials, resulting in moderate yellowish-brown colors throughout the scene.

The work from J. N. Maki et al. (1999) demonstrated the use of chromaticity scatterplots as a way to interpret and separate the colors and mixtures of materials at a landing site. All three previously published works showed that the surface of Mars is broadly yellowish-brown in color, with only a small color variability at local scales.

1.3. InSight Lander Cameras

The InSight lander is equipped with two cameras: the Instrument Context Camera (ICC) and the Instrument Deployment Camera (IDC), both described in J. N. Maki et al. (2018). The ICC is fixed-mounted to the lander body and is pointed toward the instrument deployment workspace area located to the south of the lander. The IDC is mounted to the robotic arm and can be pointed to particular areas and targets of interest. Both cameras have Bayer-pattern color filter arrays (CFAs), with individual pixel-sized red, green, and blue filters arranged in a repeating pattern (Bayer, 1976). After image acquisition, individual images are transferred from the camera into the lander computer, where they are demosaiced into color triplets and JPEG-compressed before being sent to Earth. Upon receipt at Earth the images are decompressed and stored as raw RGB images. For more information on the InSight lander cameras, see J. N. Maki et al. (2018).

1.4. Color Measurements

The InSight color cameras measure color by sampling three broad spectral channels: Red, Green, and Blue (RGB). This type of spectral measurement is called a tristimulus measurement, with the camera essentially acting as a three-channel, broadband spectrometer. The modern system of tristimulus colorimetry began with Maxwell (1860) and forms the underpinning for modern color imaging systems. The three spectral bandpasses of a color camera are broadly similar to that of the human eye, with a blue band from 400 to 500 nm, a green band from 500 to 600 nm, and a red band from 600 to 700 nm. A measurement from an RGB tristimulus system can be converted to a set of three numbers called XYZ tristimulus values, as defined by the 1931 International Commission on Illumination (Commission Internationale de l'Eclairage, or CIE). The XYZ tristimulus values represent the human response to red (X), green (Y), and blue (Z) colors, with the green channel (Y) also representing luminance (brightness). The CIE XYZ values have the advantage of being independent of the device that acquired the measurement. Data from any RGB camera system can be converted to device-independent CIE XYZ colorspace. Once converted to the CIE XYZ colorspace, measured colors from two different camera systems can be directly compared.

Because the brightness of an object affects the human perception of color, it is often convenient to separate the brightness information from the color information. This can be done by converting CIE XYZ data into chromaticity (xy) and luminance (Y), or xyY values. In this system, the color information can be plotted as an xy chromaticity coordinate in a 2-dimensional Cartesian coordinate system that is, independent of brightness. The x and y chromaticity values range from 0 to approximately 0.8, with blue being on the lower left ($x = 0.1, y = 0.1$), green in the upper left ($x = 0.1, y = 0.8$), and red in the lower right ($x = 0.7, y = 0.2$). These three points form the approximate boundaries of a region that represents the full color gamut of human vision. Direct comparisons of color can be made in this colorspace, independently of the measurement devices, the display devices, or the scene brightness. By converting the InSight color information to CIE xy chromaticity space, the InSight measurements can be directly compared to other published CIE xy chromaticity values of Mars. For more information on colorimetry and color science, the reader is directed to Wyszecki and Stiles (1982) or Hunt (1995). This study focuses on the derivation of calibrated CIE chromaticity values as measured by the InSight lander cameras, a description and summary of the results, and the comparison of the chromaticity values measured by the InSight cameras with other published measurements.

1.5. InSight Color Calibration and Processing

1.5.1. iRGB to XYZ

InSight camera images contain RGB brightness values of the red, green, and blue pixels recorded as a set of digital number (DN) values in the colorspace of the instrument (iRGB). The iRGB values represent the

instrument response to the incoming signal in the three color bands. To properly interpret or render the iRGB values on a display device, iRGB pixel values must be converted to a more standard colorspace.

InSight colorspace conversions were performed by multiplying the linear brightness values of the iRGB images by a 3×3 color conversion matrices. The coefficients for the conversion matrices were derived from prelaunch laboratory images of a color reference chart acquired with a calibrated illumination source by J. N. Maki et al., (2018). The matrix conversions described here were implemented in the InSight mission ground processing software by Abarca et al. (2019).

The relationship between raw InSight camera images (iRGB, denoted by R_i , G_i , B_i) and XYZ tristimulus values is given by:

$$\begin{bmatrix} X \\ Y \\ Z \end{bmatrix} = \begin{bmatrix} a & b & c \\ d & e & f \\ g & h & i \end{bmatrix} \begin{bmatrix} R_i \\ G_i \\ B_i \end{bmatrix} \quad (1)$$

where the matrix notation corresponds to the following linear transformation of the pixel values:

$$X = aR_i + bG_i + cB_i \quad (2)$$

$$Y = dR_i + eG_i + fB_i \quad (3)$$

$$Z = gR_i + hG_i + iB_i \quad (4)$$

The measured matrix coefficient values for the iRGB to XYZ conversion (for both the IDC and ICC cameras) are:

$$\begin{bmatrix} 1.0875708 & -1.4314745 & 3.2392806 \\ 0.17009690 & 0.93876829 & 0.37937771 \\ -0.62922341 & -4.3906116 & 15.291394 \end{bmatrix} \quad (5)$$

As noted by J. N. Maki et al. (2018), before being returned to Earth the raw InSight images were encoded nonlinearly with a gamma value of 2.2. Additionally, the blue channel of the images was scaled up by a factor of 1.718 onboard the lander prior to demosaicking of the Bayer pattern. Prior to converting to the iRGB images to the XYZ colorspace, the gamma-encoded images were converted back to a linear brightness space and the blue channel was scaled down by dividing the blue channel by 1.718.

1.5.2. Conversion to xyY (Chromaticity and Brightness)

Chromaticity is a compact way to encode color data, and this encoding scheme stores the color data in a way that is independent of brightness. The xy values form the chromaticity pair of an xyY image, with the brightness values (Y) identical to the Y channel in the XYZ image. The brightness value (denoted by a capital Y) is distinct from the y chromaticity value (lower case y). Both the XYZ and xyY colorspace and notations are CIE standards.

The XYZ data described in the previous section were converted to xy chromaticity coordinates by normalizing the X and Y tristimulus values by applying the following operations:

$$x = \frac{X}{X + Y + Z} \quad (6)$$

$$y = \frac{Y}{X + Y + Z} \quad (7)$$

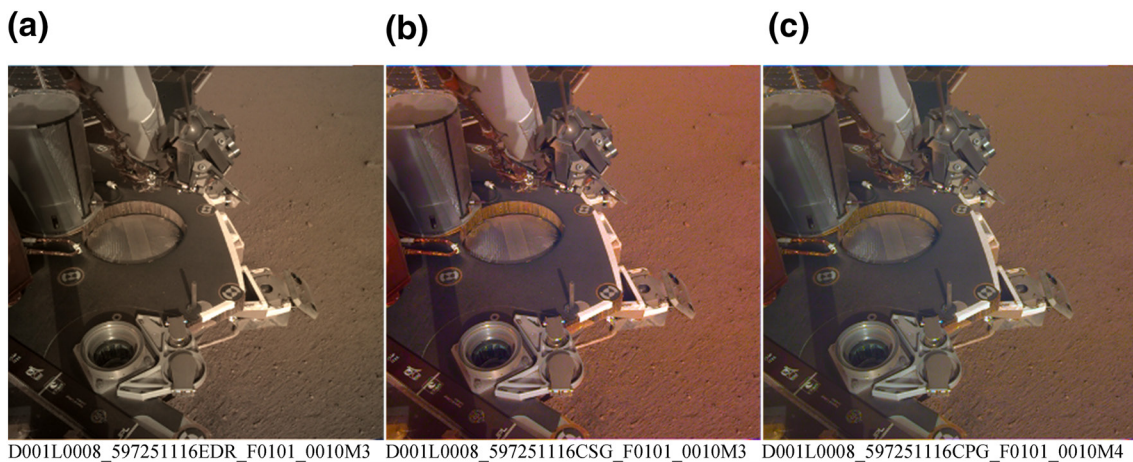


Figure 2. The visual difference between (a) iRGB (raw, no correction), (b) sRGB with no white balance, and (c) white-balanced sRGB images. This image was acquired at 15:30 local true solar time.

1.6. XYZ to sRGB

While the XYZ and xyY images are useful for directly measuring the chromaticity, to correctly render an image on a color display device it is typically converted to the sRGB colorspace (Pascale, 2003). This conversion was done using the same method used in the conversion from iRGB to XYZ.

The conversion from XYZ to sRGB was performed using a 3×3 conversion matrix:

$$\begin{bmatrix} R_s \\ G_s \\ B_s \end{bmatrix} = \begin{bmatrix} j & k & l \\ m & n & o \\ p & q & r \end{bmatrix} \begin{bmatrix} X \\ Y \\ Z \end{bmatrix} \quad (8)$$

where the matrix notation corresponds to the following linear transformation of the pixel values:

$$R_s = jX + kY + lZ \quad (9)$$

$$G_s = mX + nY + oZ \quad (10)$$

$$B_s = pX + qY + rZ \quad (11)$$

The values for the XYZ to sRGB conversion coefficients in the conversion matrix are standardized as part of the International Electrotechnical Commission (IEC) sRGB specification (IEC, 1999). These values are:

$$\begin{bmatrix} 3.2406255 & -1.537208 & -0.4986286 \\ -0.9689307 & 1.8757561 & 0.0415175 \\ 0.0557101 & -0.2040211 & 1.0569959 \end{bmatrix} \quad (12)$$

1.7. White Balancing of sRGB Images

Because the Martian sky adds a yellowish-brown color to the overall scene, white materials appear as a yellowish-brown white in the sRGB images. This yellowish-brown color cast can be removed by performing a white balance operation on the sRGB image data. White balancing renders white objects in the scene as white objects in the image, regardless of the illuminant. Under different illuminants, the measured chromaticity (xy) values of the white material may differ, but the white material in a white-balanced sRGB image

appears as white to a viewer regardless of the illuminant. Figure 2 shows an example of a white-balanced InSight sRGB image.

The white balancing of InSight images was performed by applying a 3×3 matrix with three nonzero coefficients along the diagonal:

$$\begin{bmatrix} R_w \\ G_w \\ B_w \end{bmatrix} = \begin{bmatrix} s & 0 & 0 \\ 0 & t & 0 \\ 0 & 0 & u \end{bmatrix} \begin{bmatrix} R_s \\ G_s \\ B_s \end{bmatrix} \quad (13)$$

where the matrix notation corresponds to the following linear transformation of the pixel values:

$$R_w = sR_s \quad (14)$$

$$G_w = tG_s \quad (15)$$

$$B_w = uB_s \quad (16)$$

where R_s , G_s , and B_s are the nonwhite balanced, linear input pixel values and R_w , G_w , and B_w are the resultant white-balanced linear pixel values.

The white balance coefficients for InSight sRGB images were derived from postlanding images of white patches on the camera calibration target, white paint on the InSight lander, and white paint on the lander robotic arm. The derived values for InSight sRGB white balance coefficients are:

$$\begin{bmatrix} 0.7965 & 0 & 0 \\ 0 & 1.0 & 0 \\ 0 & 0 & 2.3038 \end{bmatrix} \quad (17)$$

As a final step, a gamma correction of 2.2 was reapplied to the linear sRGB images to bring out contrast in the darker areas of the image. The images in Figure 2 show three types of color images: iRGB, sRGB, and white-balanced sRGB. The iRGB image (panel a, left) has minimal color saturation, intended to preserve luminance information while keeping noise to a minimum. The sRGB image (panel b, center) renders the colors as measured by the camera. The white-balanced sRGB image (panel c, right) renders the white edges of the lander as white.

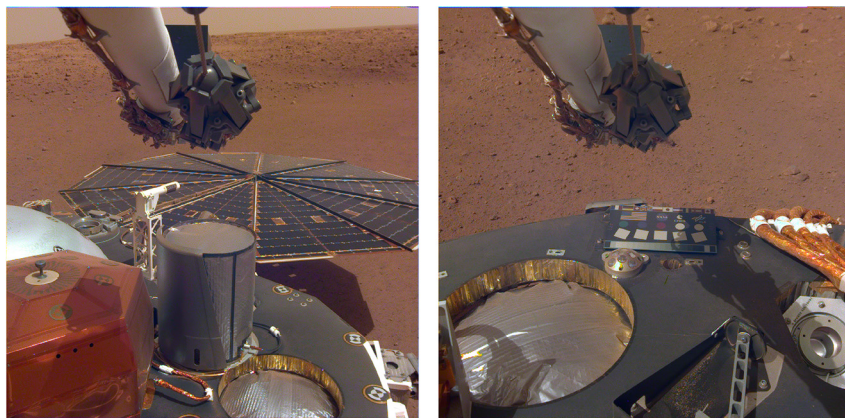
2. Results

2.1. Image Data Sources

The best sources of InSight color data are the IDC images acquired during the early part of the mission (approximately sols 8–20). During this period the camera lenses were relatively free of dust, the lander deck and camera calibration target were relatively clean, and the ground around the landing site had been recently dusted off by the lander rocket engines. Images acquired during this early phase have high contrast, indicating that the cameras had not yet acquired significant dust layers on the front lenses.

2.2. Calibrated Color Images

All of the InSight IDC and ICC images have been color-calibrated using the method described in the previous section. Results of this work are provided in Figures 3–8 as a set of reference images for color-calibrated images of the Martian surface. Unless stated otherwise, the example images are white-balanced, sRGB images with an applied gamma correction of 2.2.



D005L0010_597414005CPG_F0002_0080M2 D000M0012_597599441CPG_F0000_0129M2

Figure 3. Color-calibrated images of the lander top deck and far field terrain. The light yellowish brown colors indicate fine ferric oxide dust, while the darker yellowish brown are mixtures of dust and granular basaltic material. The image product names are listed below each image.

3. Chromaticity Analysis

3.1. Methodology

All of the InSight images received from Mars were converted into color-calibrated, three-channel xyY images, using the process described in the previous section. The first channel of the xyY image contains the x chromaticity values, the second channel contains the y chromaticity values, and the third channel contains the luminance (Y) values.

For the figures in this section, a rectangular region of interest within an image was chosen visually by designating the pixel coordinates of the upper left and lower right of the rectangle. The chromaticity values from the selected region of interest were plotted as individual data points in an xy scatterplot. The chromaticity coordinate for the entire region was calculated by computing the mean average of all points within the region. The standard deviation (1σ) of the x and y chromaticity points along each axis were calculated individually, σ_x and σ_y , and were used as an estimate of the dispersion of the chromaticity points.



D000M0008_597249029CPG_F0000_0552M2 D000M0008_597249595CPG_F0000_0555M2

Figure 4. Color-calibrated IDC images of the near field terrain in front of the lander. These near field images show the distinct gray/dark gray color of the granular material (composed of basaltic rock fragments) against the finer dust material, which appears as a yellowish brown color. The dark gray basaltic grains in the image on the right were exposed (dust blown off) by the lander descent rockets.



Figure 5. Color-calibrated IDC images of the area underneath the lander. These images show large blocks of basaltic material, appearing as a dark gray color, covered with a fine layer of yellowish brown dust. Dust appears as a bright yellowish brown material in this image, particularly on the lander legs. The mixtures of the basaltic grains and dust appear as a moderate yellowish brown material. The faint purple hues in some areas of the surface in these images are due to scattered light and chroma noise from the camera, and are not coming from the surface materials in the scene (exceptions include the lander rocket nozzles, which are multicolored).

To aid in the reporting of the chromaticity values, the measured points were also approximated as an ellipse, with the ellipse center at the mean average of the data points. The semi-major and semi-minor axes of the ellipse were determined by the 1σ values, σ_x and σ_y , rotated by an angle (θ). The semi-major axis of the ellipse is given by:

$$a = \sqrt{(\sigma_x)^2 + (\sigma_y)^2} \quad (18)$$

and the semi-minor axis was calculated as:

$$b = \sigma_x \sin \theta \quad (19)$$

The rotation angle of the ellipse was calculated as:

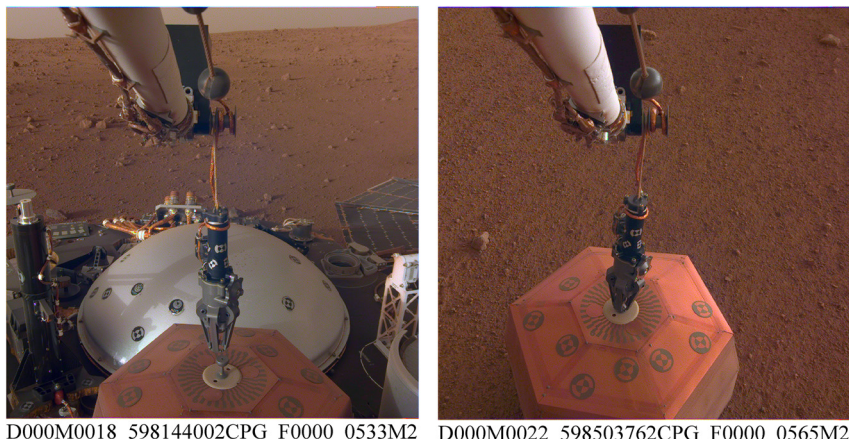
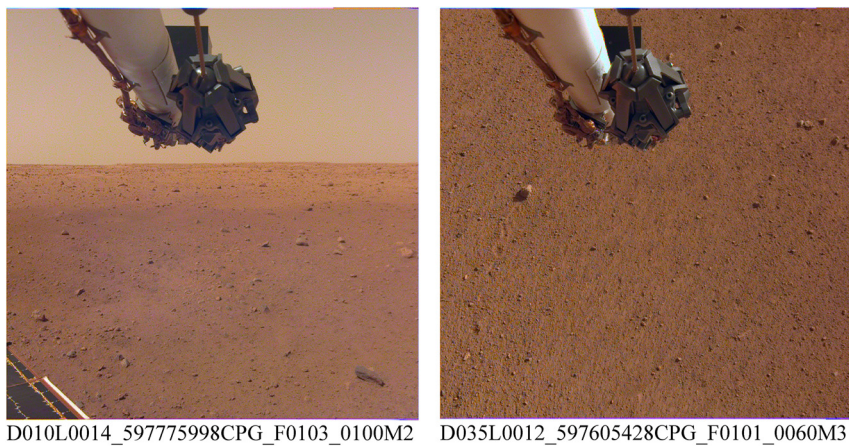


Figure 6. Examples showing how the illumination at different times of day affects the appearance of colors. The image on the left was acquired at 17:34 local mean solar time, and the image on the right (illuminated purely by skylight) was acquired postsunset at 18:52 local mean solar time. The postsunset image shows a slightly redder hue due to the color of the diffuse sky brightness. Fine layers of dust on the rocky materials give the rocks a bright yellowish brown color.



D010L0014_597775998CPG_F0103_0100M2 D035L0012_597605428CPG_F0101_0060M3

Figure 7. Images of the far-field (left) and mid-field (right) terrain. The far-field images show a brightness discontinuity at a radial distance of approximately 20 m from the lander. This discontinuity was created when the brighter, yellowish brown dust was blown off of the underlying basaltic material during the landing event. The color of the near field terrain on the right matches the color of the near field terrain on the left. The material past 20 m has a slightly more yellowish brown color due to the dust layer.

$$\theta = \tan^{-1} \frac{\sigma_y}{\sigma_x} \quad (20)$$

The figures in Sections 3.2–3.4 each have two panels. Panel a, on the left, shows the color-calibrated image. Within the image, the selected region of interest is outlined by a black rectangle. Panel b, on the right side, shows the chromaticity scatterplot of all the pixels contained within that region of interest, along with additional chromaticity points for reference.

3.2. Mars Daylight

The chromaticity of Mars daylight was measured on Sol 12 using a white patch on the InSight camera calibration target. The chromaticity of an illuminated white patch is also referred to as the white point of that

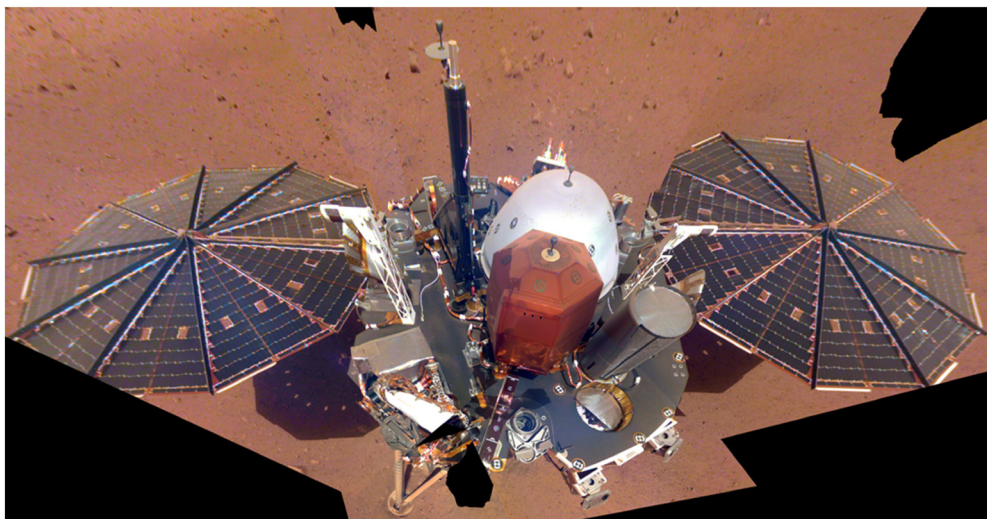


Figure 8. Calibrated color images mosaicked together, showing the lander top deck on Sol 8. Other calibrated color mosaics can be found in Golombek et al. (2020). The white material on the lander deck, including the calibration target and white paint, serve as a white reference point.

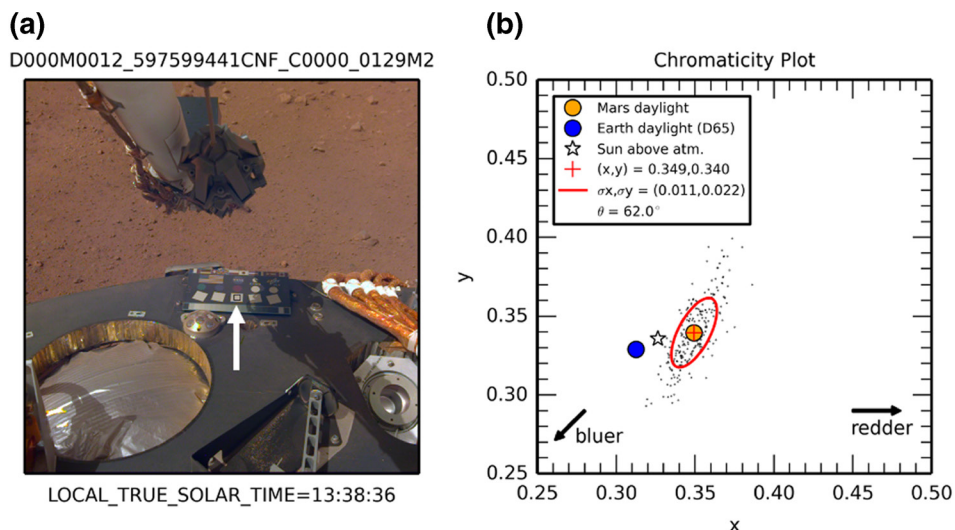


Figure 9. Chromaticity of Mars daylight, measured directly from a white patch on the IDC calibration target. The region of interest is denoted by the white arrow in panel (a). Mars daylight includes illumination from direct sunlight and diffuse skylight.

illuminant. The chromaticity of the white patches on the calibration target were verified in the laboratory prior to launch using a calibrated 3,000 Kelvin incandescent light source. The white patches have a matte finish and are approximated as Lambertian reflectors. The camera calibration target is described in more detail in J. N. Maki et al. (2018).

The white point of Martian daylight was measured by averaging the xy chromaticity pixel values within a white patch on the calibration target. The measured values are $x = 0.35$, $y = 0.34$ (standard deviations of $\sigma_x = 0.01$ and $\sigma_y = 0.02$), as shown in Figure 9. This white point corresponds to a redder color than Earth daylight (CIE illuminant D65, $x = 0.31$, $y = 0.33$) by approximately ($\delta x = 0.04$, $\delta y = 0.01$). The Mars white point value was also measured from white painted areas on the lander and verified to match the values from the white patches on the calibration target.

Mars daylight includes contributions from two main sources: direct solar illumination and diffuse illumination from the sky. The white point measurement includes contributions from both of these illumination sources. Although we cannot rule out the possibility that a thin layer of dust is reddening the target slightly and influencing the white point measurement, we estimate that this effect is negligible based on visual inspection of the images.

The chromaticity scatterplot in Figure 9 shows all of the data points in the region of interest inside the center white patch. The chromaticity coordinate of pure sunlight, a 5,778 K blackbody at the top of the atmosphere, is $x = 0.326$, $y = 0.336$ and is represented by the white star in panel (b). The chromaticity of Earth daylight, bluer than pure sunlight, is shown as a blue circle. The chromaticity of Mars daylight, redder than pure sunlight, is shown as a yellowish-brown circle. The scatterplot shows how Martian daylight is on the red side (right side) of pure sunlight, while Earth daylight is on the blue side (left side) of pure sunlight. In addition to enabling white balancing, the result in Figure 9 could be used to render outdoor Earth images as outdoor Mars images by shifting the Earth image in chromaticity coordinates toward red by $\delta x = 0.04$ and toward yellow by $\delta y = 0.01$. This technique would allow a more direct comparison of the color properties of terrestrial materials with images of Martian materials, as both images would be in the same colorspace.

The chromaticity of a shadowed white patch on the target is similar to the chromaticity of the unshadowed region, only separated by ($\delta x = 0.005$, $\delta y = 0.003$). Figure 10 shows the sampled region of a shadowed area of the calibration target.

The chromaticity of the Martian sky above the horizon is shown in Figures 11 and 12. Although acquired 2 h apart, the chromaticity measurements are similar. At higher elevations, the color of the sky becomes less

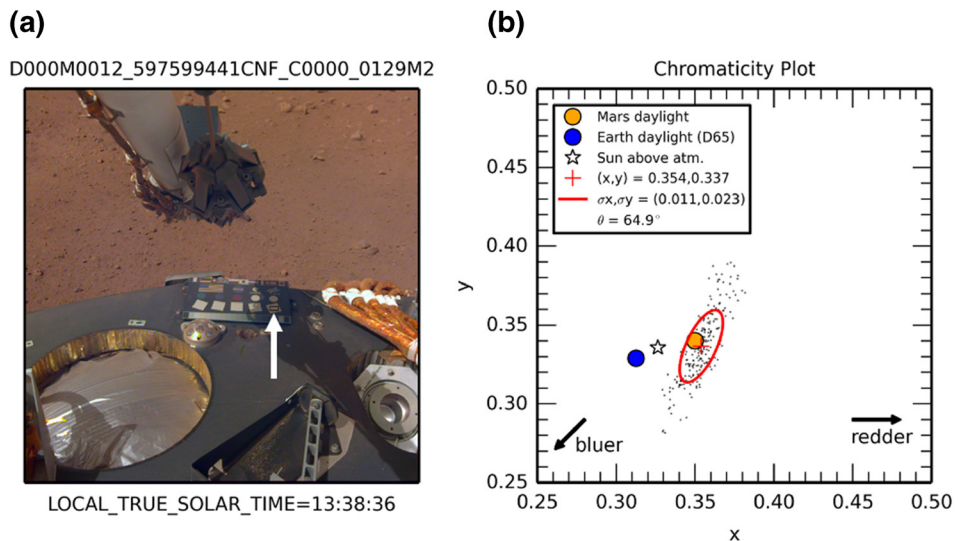


Figure 10. Chromaticity of Mars diffuse skylight only, with no direct illumination. The diffuse skylight is measured from a shadowed white patch, denoted by the white arrow in panel a.

red. Figure 13 shows the chromaticity of the sky at an elevation of 77° above the horizon, measured from an image acquired on Sol 18. The corresponding sRGB image in Figure 13 is a grayish-brown and not the yellowish-brown color seen near the horizon, as shown in Figures 11 and 12.

3.3. Chromaticity of Martian Terrain

The measured chromaticity of the terrain around the lander show yellowish brown colors, with an average xy chromaticity of the Martian terrain measured at $x = 0.42$ and $y = 0.36$, with standard deviations of $\sigma_x = 0.02$ and $\sigma_y = 0.03$. Figure 14 shows the measured chromaticity of a representative area of the terrain to the north of the lander. The chromaticity of the terrain in Figure 14 matches the chromaticity the terrain beyond 20 m from the lander (Figure 15). Because the area farther from the lander was less disturbed by the lander rocket plumes, the color is slightly redder ($\delta x = 0.02$ and $\delta y = 0.01$, due to a thicker dust layer) than the mid-field terrain in Figure 16. However, the visual discontinuity between the appearance of the two

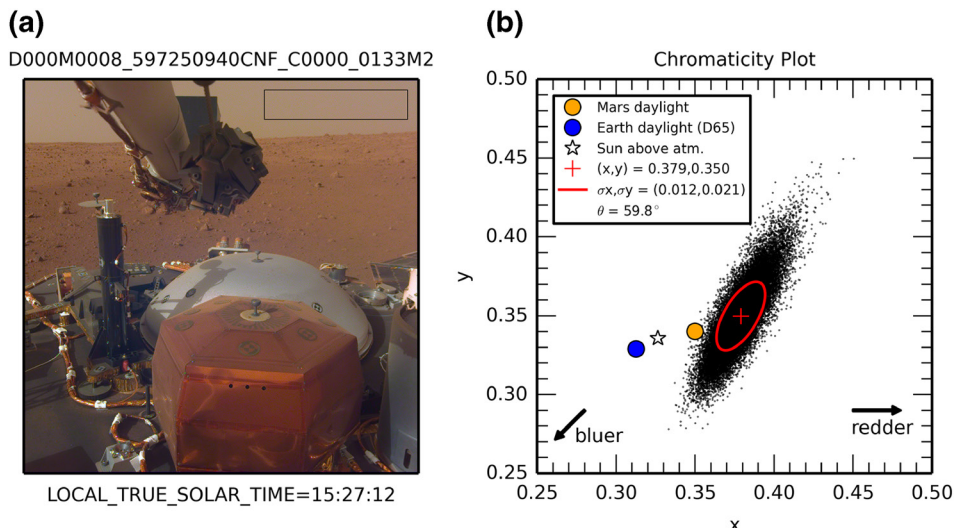


Figure 11. Chromaticity of the Martian sky near the horizon, looking north from the lander (9° east of north). The angle between the sun and the sky patch in this image is approximately 230° .

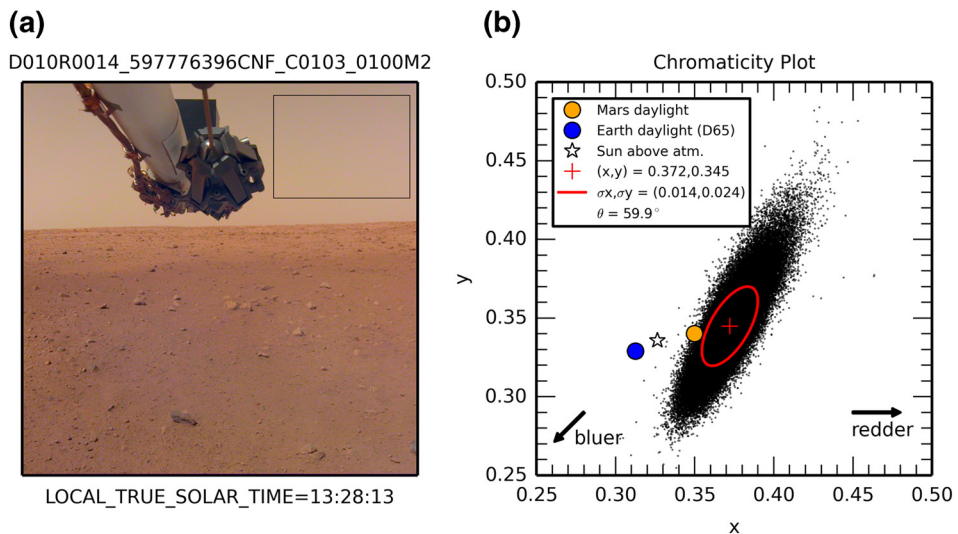


Figure 12. Chromaticity of the Martian sky near the horizon, looking due north of the lander, acquired 2 h earlier in the day than the image in Figure 11. The angle between the sun and the sky patch in this image is approximately 150° .

regions is mainly due to the brightness difference. The chromaticity of the near-field terrain, which contains a mixture of dust and rocks, is shown in Figure 17. It matches the general chromaticity of the landing site as shown in Figures 14 and 15.

3.4. Rock Chromaticity

During the InSight landing event, the lander rockets blew away the dust immediately below the lander and appeared to have overturned some of the smaller rocks. Figure 18 shows one of these rocks, which visually appears to be relatively free of dust. This relatively clean rock has a chromaticity value of $x = 0.32$, and $y = 0.32$, with a standard deviation of approximately $\sigma_x = 0.02$ and $\sigma_y = 0.03$. Because the rock chromaticity is within $\delta x = 0.01$ and $\delta y = 0.02$ of the chromaticity of pure sunlight,

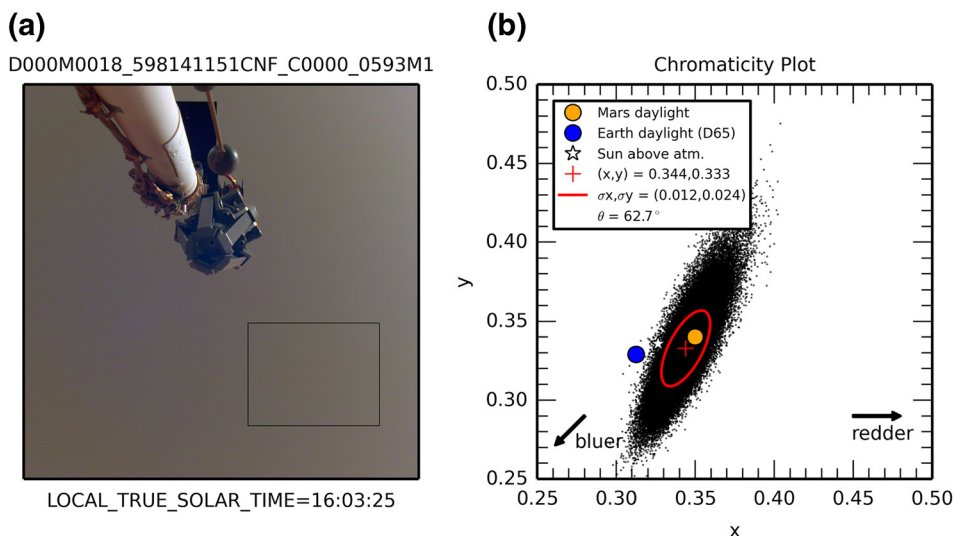


Figure 13. Chromaticity of the sky, looking approximately 77° above the horizon. This sky at this elevation is bluer than the sky near the horizon ($\delta x = -0.03$ and $\delta y = -0.01$), and exhibits a characteristically brownish gray color, consistent with previous measurements from J. N. Maki et al. (1999). The angle between the sun and the sky patch in this image is approximately 120° .

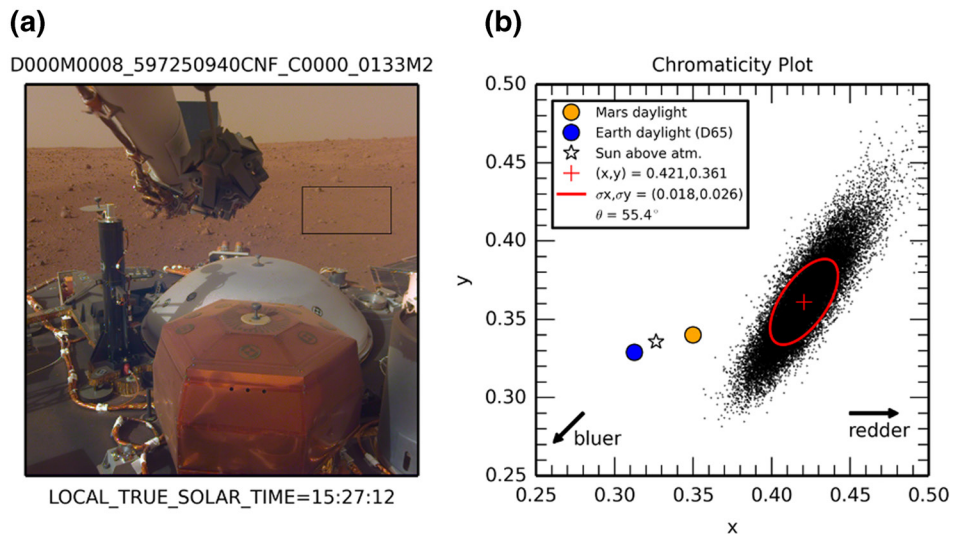


Figure 14. Chromaticity of a patch of terrain located to the north side of the InSight lander.

the color of the rock is a gray color, suggesting a spectrally neutral reflectance profile as a function of wavelength.

3.5. Luminance and Brightness Measurements

In addition to the chromaticity information, the xyY and XYZ images also record the scene brightness. The luminance information corresponds to the brightness in the green channel of the camera. Although not calibrated in absolute units, the linear brightness values within an image can be used to determine relative brightness. Note that the term luminance refers to the brightness of a scene in the green (Y) channel, as measured by the human eye. In the context of this work the luminance and brightness are considered equivalent, i.e., the DN values of the X, Y, and Z channels of an XYZ image all represent linear brightness in a scene. The units of the InSight luminance channel are arbitrary, and in this case were chosen to ensure that exposure-corrected images fit within the range of a 16-bit integer.

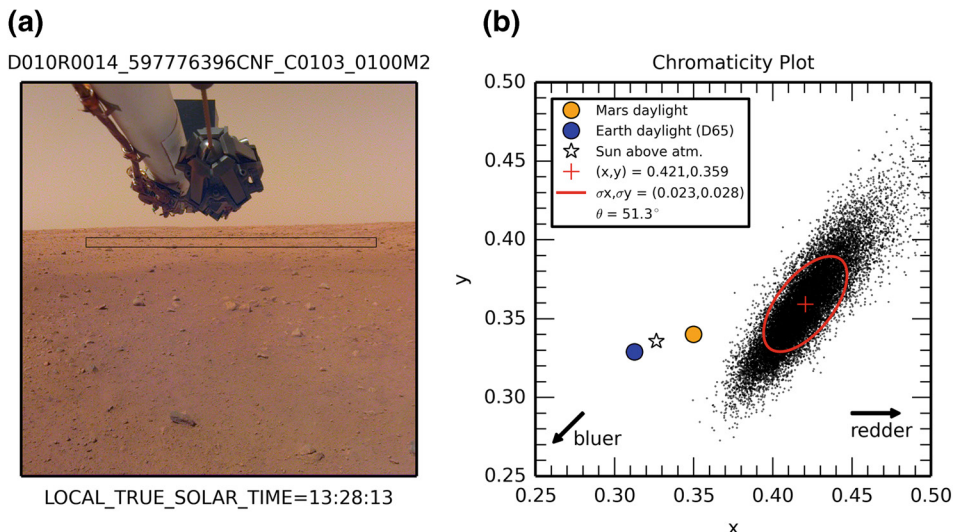


Figure 15. Chromaticity of the far field, brighter terrain at the InSight landing site.

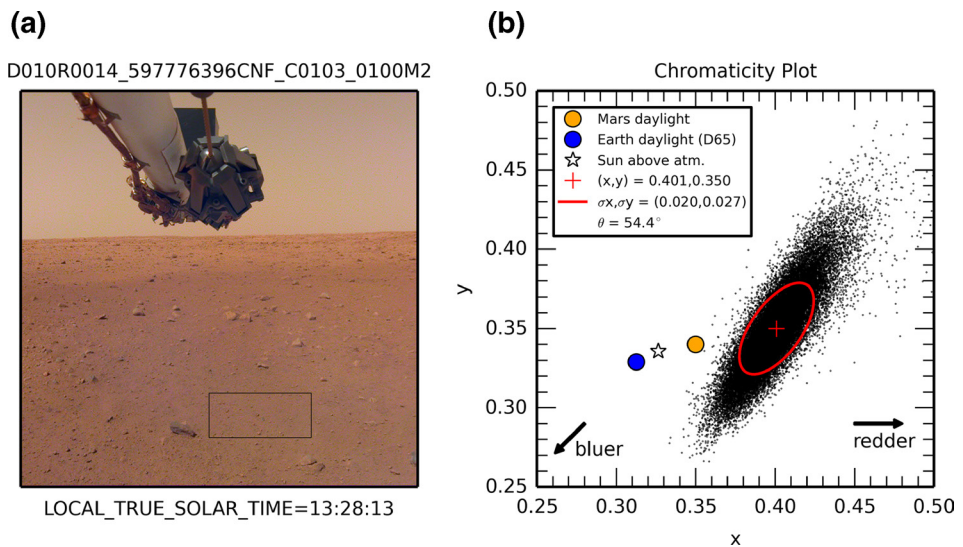


Figure 16. Chromaticity of darker, mid-field terrain at the InSight landing site.

3.5.1. Direct Illumination Versus Diffuse Illumination

As discussed in Section 3.2, Mars daylight is comprised of two components: (1) direct illumination by sunlight and (2) diffuse illumination by Mars skylight. The relative contributions of these two components can be measured directly by examining the luminance channel of the calibrated XYZ images. Figure 19 shows the IDC calibration target, partially shadowed. By measuring the sunlit regions (direct + diffuse) and the shadowed regions (diffuse only), it is possible to infer the direct illumination by subtracting the diffuse illumination from the total (direct + diffuse) illumination. The relative percentage of direct versus diffuse illumination changes diurnally and seasonally, and is also a function of the dust optical depth (τ).

The Sol 12 measurements of the calibration target indicate a diffuse sky brightness contribution of approximately 36%, with direct sunlight contributing the other 64%. The ratio of diffuse to direct illumination is 56%. The dust optical depth on InSight Sol 12 is estimated to be approximately $\tau = 0.8$ (Banfield et al., 2020), and the direct fraction of 64% is consistent with the measurements of Kinch et al. (2007) for similar optical

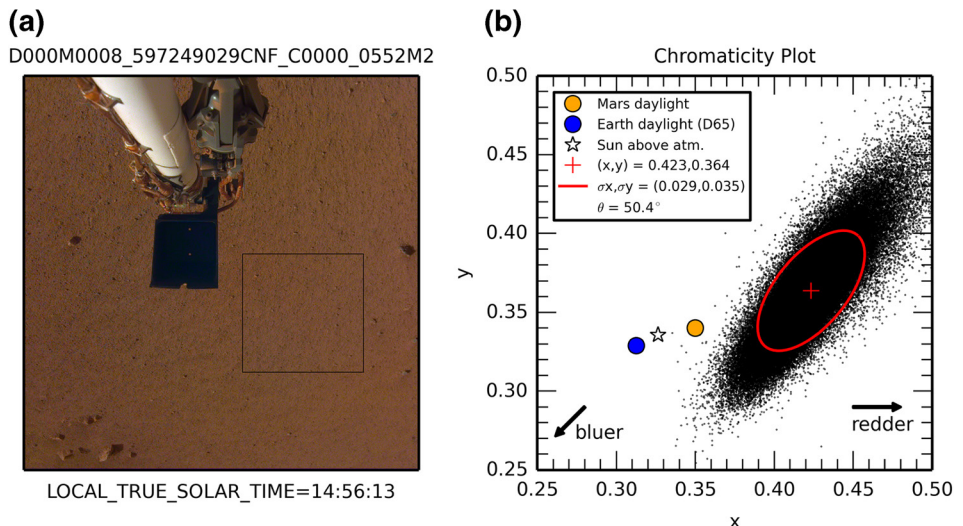


Figure 17. Chromaticity of a patch of soil near the lander.

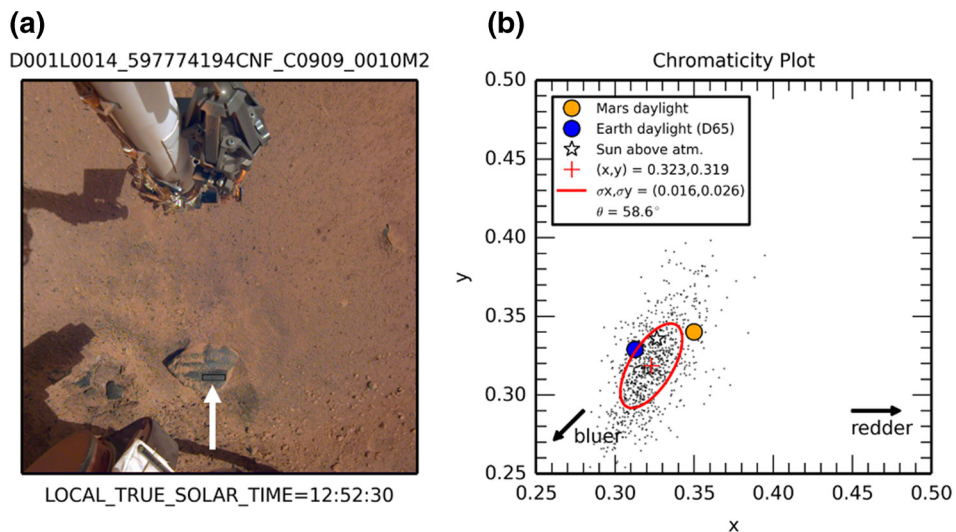


Figure 18. Chromaticity of a patch of rock material in direct sunlight, mostly cleaned of dust by the lander rocket engines.

depths. The diffuse to direct ratio is also consistent with measurements of Smith et al. (1997a), who measured a diffuse/direct illumination ratio of 40% under a correspondingly lower optical depth ($\tau = 0.5$).

3.5.2. Relative Brightness of Terrain

As discussed in Section 3.3, the bright/dark visual discontinuity of the terrain located ~ 20 m away from the lander shows a small color difference between the bright and dark terrain, with the brighter terrain appearing as slightly redder ($\delta x = 0.02$ and $\delta y = 0.01$). In addition to the color change, the brightness of these two regions is also different, and is the more dominant visual effect of the two. Figure 20 shows that the darker region is approximately 25% darker than the brighter region in the red and green channels, and

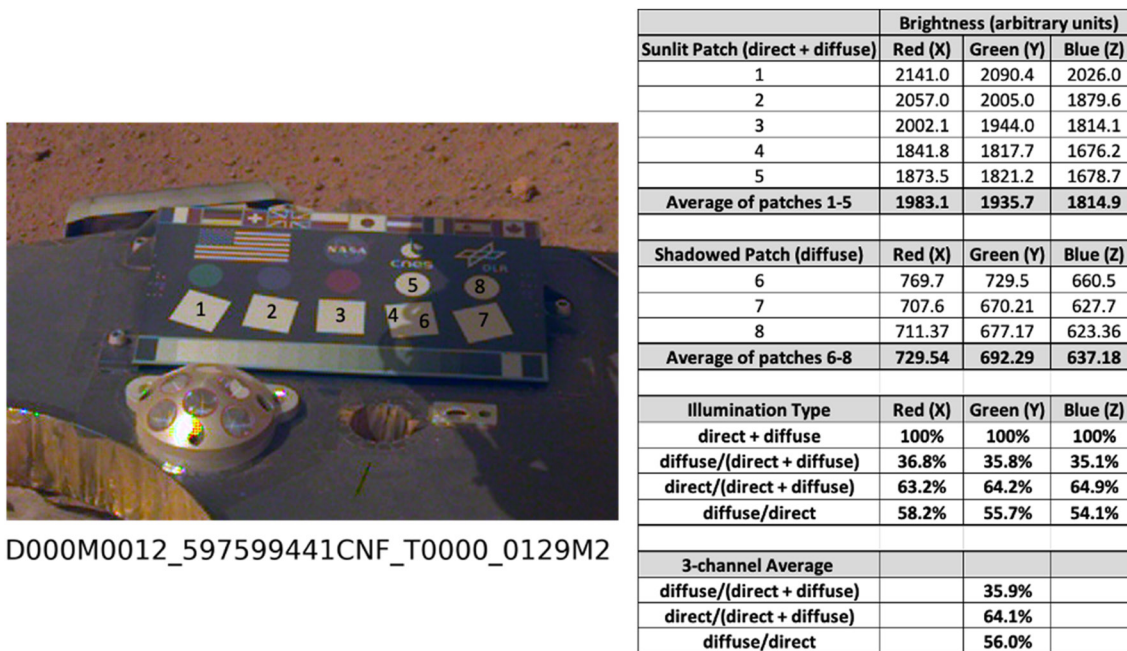


Figure 19. Measurement of direct versus diffuse illumination on the InSight calibration target. Patches 1–5 are sunlit regions. Patches 6–8 are shadowed regions. This calibration target image was acquired at 13:38 local true solar time.

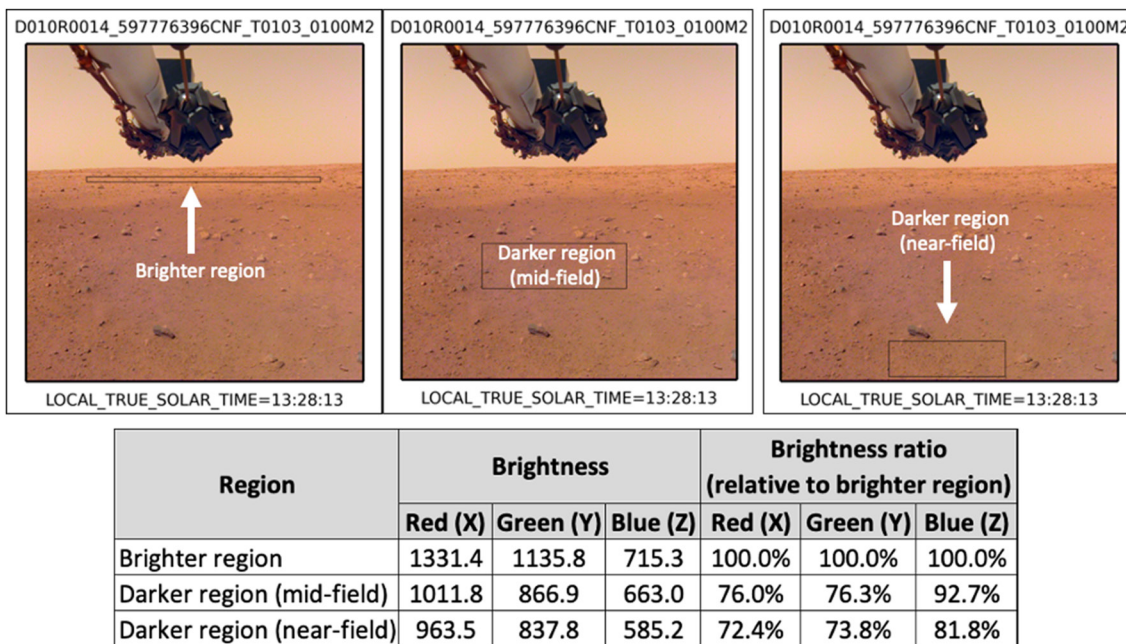


Figure 20. Relative brightness of the darker and brighter terrains near the lander. The red and green channels show an approximately 25% reduction in brightness in the darker areas affected by the lander rockets. The brightness units are linear, with an arbitrary absolute scale.

only ~8%–20% darker in the blue channel, depending on the distance from the camera. The 25% measured value differs slightly from the reported estimate of 35% from orbit (Golombek et al., 2020). The reason for this difference is not entirely understood, but is likely due to the differences in viewing angle between the overhead orbiter view and the view from the lander camera, which views the terrain more obliquely. If the top (horizontal) surfaces of the rocks were cleaned of dust more efficiently than the sides (vertical), the orbiter would see a larger change in brightness than the lander cameras, which view more of the sides of materials than the orbiter.

4. Discussion

4.1. Summary of Results

The chromaticity results of this work are summarized in Table 1. Included in this table are the standard deviation values (1σ) for both the x and y chromaticity coordinate. The 1σ values are introduced in this work to help better characterize the dispersion of chromaticity points within the selected regions.

4.2. Spectral Mixing and Chromaticity Endpoints

As shown Huck et al. (1977) and J. N. Maki et al (1999), the observed chromaticities at Mars landing sites are mixtures of rock and soil, modified by Mars daylight. InSight data also show a similar dispersion (as illustrated in Figure 21), with the Martian sky on the left side (less red), the rocky material in the center, and the dustier material on the right (more red).

The InSight measurement of the clean rock in Figure 18 provide a possible lower-left bound (blue side) on the chromaticity scatterplot at

Table 1
Summary of Chromaticity Analysis in This Work

Scene type	Figure	x	y	σx	σy
Daylight	9	0.349	0.340	0.011	0.022
Diffuse skylight	10	0.354	0.337	0.011	0.023
Sky 1	11	0.379	0.350	0.012	0.021
Sky 2	12	0.372	0.345	0.014	0.024
Sky 3 (high elevation)	13	0.344	0.333	0.012	0.024
Terrain 1	14	0.421	0.361	0.018	0.026
Terrain 2 (far field, brighter)	15	0.421	0.359	0.023	0.028
Terrain 3 (mid-field)	16	0.401	0.350	0.020	0.027
Terrain 4 (near-field)	17	0.423	0.364	0.029	0.035
Rock	18	0.323	0.319	0.016	0.026

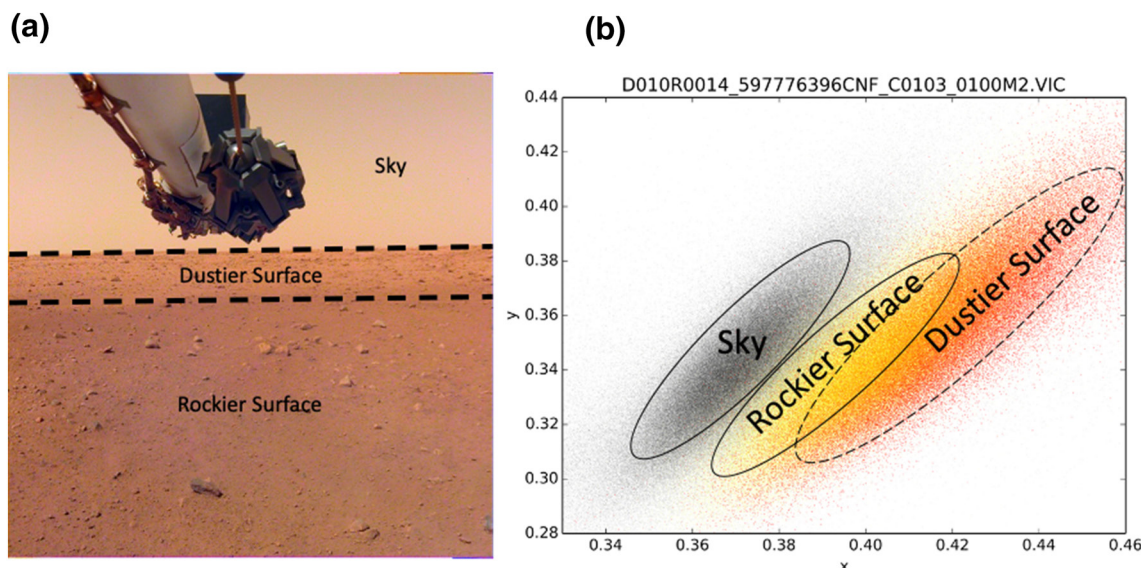


Figure 21. The chromaticity points of the entire image in panel a plotted as a chromaticity scatterplot (shown in panel b). The chromaticities in the image come from three spectral endpoints: sky (shown as black points), rocks (shown as yellow points), and dust (shown as orange points).

($x = 0.32, y = 0.32$). The middle region of the scatterplot represents varying degrees of dust/rock mixtures with characteristic yellowish-brown colors, and an average chromaticity value of approximately ($x = 0.42, y = 0.36$). The upper-right (red/yellow) side of the chromaticity scatterplot is probably pure dust.

Although the dust cannot be resolved by the lander cameras, the color of the dust can be inferred from the chromaticity scatterplot. The upper right of the chromaticity plots in Figures 14 and 15 are located approximately 3σ away from the mean, corresponding to approximately ($x = 0.474, y = 0.435$), suggesting that pure dust might have this color.

Material on the other end of the diagonal, located 3σ away from the mean, in Figures 14 and 15 (lower left) would suggest a pure rock chromaticity value of ($x = 0.366, y = 0.285$). Interestingly, this value does not match the directly measured xy chromaticity value of the clean rock ($x = 0.32, y = 0.32$) in Figure 18. This could suggest that the lower left endpoints in Figures 14 and 15 are not representative of pure rock material, but instead are mixtures of rocky material and dust. If true, this suggests that virtually all of the rocky material in the natural terrain is covered by a thin, reddening dust layer, which reddens the rock and shifts the chromaticity of the rocks to the right by $\delta x = 0.04$. The y chromaticity difference between the clean rock and the blue endpoint of the scatter plot is $\delta y = 0.035$, and is not well understood. One interpretation could be that the clean rock in Figure 18 may have some residual dust on it, not resolved by the camera but contributing to the color by yellowing it.

4.3. Chroma Noise in InSight Camera Images

The InSight cameras were inherited as flight spare cameras from the Curiosity Rover mission (J. Maki et al., 2012). The InSight project upgraded the detectors from grayscale to color by adding a Bayer color filter array layer to the detector stack. The resultant cameras, while color-capable, have a very low blue sensitivity (see Figure 6 in J. N. Maki et al., 2018). Because of this low blue sensitivity, when converting from the instrument colorspace (iRGB) to the XYZ colorspace using the steps described in Section 1.5.1, the blue channel is scaled up by a factor of 3.2 in the X tristimulus value, and a factor of 15.3 in the Z tristimulus value. This scaling amplifies the noise in the blue channel and injects additional noise into the red channel, creating chroma noise.

The chroma noise in an InSight image is distributed mostly in the purple and yellow directions in chromaticity space. In the chromaticity scatterplots, the chroma noise appears as a diagonal scatter from the lower left to the upper right, with a counterclockwise rotation angle of approximately 60° relative to the x -axis.

The noise can be seen visually as pixel-to-pixel variations, appearing as a yellow and purple speckle, in the calibrated images when viewing InSight images at the pixel level on an image display.

The chroma noise does not affect the average chromaticity values, because the scattering occurs equally on both sides (i.e., the purple and yellow sides) of the average value. However, the noise masks subtle differences between the colors of different materials. Because of this, caution should be taken when interpreting the endpoints of the InSight chromaticity scatterplots. The 1σ ellipses overlaid on the scatterplot are provided as an estimate of the true variation in chromaticity. Chromaticity points outside the 1σ ellipses are believed to be caused mostly by camera noise.

4.4. Comparison to Other Work

The measured InSight chromaticities presented in this work are consistent with those measured by Viking (Huck et al., 1977), Mars Pathfinder (J. N. Maki et al., 1999), and the MER (Bell et al., 2006). The measured InSight chromaticities show more data points in the blue/rocky range ($x = 0.37\text{--}0.40$ and $y = 0.30\text{--}0.35$) than J. N. Maki et al. (1999), the only other published values of rock chromaticities. One possible explanation for the additional blue/rocky chromaticity data points in the InSight data is that the lander rockets blew off a layer of dust during landing, revealing more of the rocky material. The Mars Pathfinder system used an airbag landing system, and thus the dust layer at the Pathfinder landing site would not have been blown off by lander rockets. Huck et al. (1977) did not publish any Viking rock chromaticity measurements.

Martian sky chromaticities are also in family with previous published values, with the sky showing the largest variability in color depending on the time of day and elevation above the horizon. The high-elevation sky image in Figure 13 reveals a chromaticity value of ($x = 0.344$, $y = 0.333$), which matches the predicted value of an atmosphere with much less dust ($\tau = 0.1$) from Bell et al. (2006). The InSight tau value during this period was reported as $\tau = 0.8$ by Banfield et al., 2020. The exact cause of this apparent discrepancy is not known, but suggests that either the dust optical depth directly above the lander may not be as high as the generally derived values, or that other scattering effects are contributing to a less yellowish-brown color above the lander.

4.5. Mars White Point

The direct measurements of the chromaticity of Martian daylight ($x = 0.349$, $y = 0.340$) presented in this work provide useful information for the proper white balancing of Mars images. The chromaticity of sunlight, represented as a 5,778 K blackbody at the top of the atmosphere, is ($x = 0.326$, $y = 0.336$). Given that the atmospheric transmission of direct sunlight through the Martian atmosphere is spectrally neutral during midday (Smith et al., 1999), the reddening of Martian daylight is caused mostly by the diffuse skylight, slightly reddened relative to the direct sunlight, mixing with the direct solar illumination.

4.6. Planetary Data System (PDS)

All of the raw images, calibrated color images, and chromaticity data described in this study are archived in the NASA PDS. The filenames of the data used in this work are shown in the figures, with the calibrated color images denoted by the “CPG” characters in the filenames, and the corresponding chromaticity data denoted by “CNF” in the filenames. All of the source data can be obtained directly by accessing the InSight Camera data set in the NASA PDS, Imaging Sciences Node (J. Maki et al., 2019).

Data Availability Statement

Data used and generated in this work can be found here: <https://doi.org/10.17189/1510487>.

References

- Abarca, H., Deen, R., Hollins, G., Zamani, P., Maki, J., Tinio, A., et al. (2019). Image and data processing for InSight lander operations and science. *Space Science Reviews*, 215(22), 1–53. <https://doi.org/10.1007/s11214-019-0587-9>

Acknowledgments

This work was performed as part of the InSight Project at the Jet Propulsion Laboratory, California Institute of Technology, under contract with NASA. This study is InSight Contribution Number 139. The authors thank the efforts of the entire InSight project.

- Banerdt, W. B., Smrekar, S. E., Banfield, D., Giardini, D., Golombek, M., Johnson, C. L., et al. (2020). Initial results from the InSight mission on Mars. *Nature Geoscience*, 13(3), 183–189. <https://doi.org/10.1038/s41561-020-0544-y>
- Banfield, D., Spiga, A., Newman, C., Forget, F., Lemmon, M., Lorenz, R., et al. (2020). The atmosphere of Mars as observed by InSight. *Nature Geoscience*, 13(3), 190–198. <https://doi.org/10.1038/s41561-020-0534-0>
- Bayer, B. E. (1976). Color Imaging Array. *United States Patent #*, 3, 971,065.
- Bell, J. F., Savransky, D., & Wolff, M. J. (2006). Chromaticity of the Martian sky as observed by the Mars Exploration Rover Pancam instruments. *Journal of Geophysical Research*, 111, E12S05. <https://doi.org/10.1029/2006JE002687>
- Bell, J. F., Squyres, S. W., Herkenhoff, K. E., Maki, J. N., Arneson, H. M., Brown, D., et al. (2003). Mars Exploration Rover Athena Panoramic Camera (Pancam) investigation: MER ATHENA PANORAMIC CAMERA INVESTIGATION. *Journal of Geophysical Research*, 108(E12), 8063. <https://doi.org/10.1029/2003JE002070>
- Ehlmann, B. L., & Edwards, C. S. (2014). Mineralogy of the Martian Surface. *Annual Review of Earth and Planetary Sciences*, 42(1), 291–315. <https://doi.org/10.1146/annurev-earth-060313-055024>
- Golombek, M., Warner, N. H., Grant, J. A., Hauber, E., Ansan, V., Weitz, C. M., et al. (2020). Geology of the InSight landing site on Mars. *Nature Communications*, 11(1), 1014. <https://doi.org/10.1038/s41467-020-14679-1>
- Huck, F. O., Jobson, D. J., Park, S. K., Wall, S. D., Arvidson, R. E., Patterson, W. R., & Benton, W. D. (1977). Spectrophotometric and color estimates of the Viking lander sites. *Journal of Geophysical Research*, 82(28), 4401–4411.
- Hunt, R. W. G. (1995). *Measuring colour* (2nd ed.). Chichester, England: Ellis Horwood.
- International Astronomical Union Working Group for Planetary System Nomenclature. (2020). *Gazetteer of planetary nomenclature*. Retrieved from <http://planetarynames.wr.usgs.gov/>
- International Electrotechnical Commission. (1999). *IEC 61966-2-1, Amendment 1, Multimedia systems and equipment – Colour measurement and management*. Retrieved from <https://www.w3.org/Graphics/Color/srgb>
- Kinch, K. M., Sohl-Dickstein, J., Bell, J. F., Johnson, J. R., Goetz, W., & Landis, G. A. (2007). Dust deposition on the Mars Exploration Rover Panoramic Camera (Pancam) calibration targets. *Journal of Geophysical Research*, 112, E06S03. <https://doi.org/10.1029/2006JE002807>
- Maki, J., Deen, R., Abarca, H., & Zamani, P. (2019). *InSight Cameras Experiment Data Record (EDR) and Reduced Data Record (RDR) Data Products Data Products Data Collection [Data set]*, Planetary Data System, Imaging Node. Retrieved from <https://doi.org/10.17189/1510487>
- Maki, J., Thieszen, D., Pourangi, A., Kobzeff, P., Litwin, T., Scherr, L., et al. (2012). The Mars Science Laboratory Engineering Cameras. *Space Science Reviews*, 170(1–4), 77–93. <https://doi.org/10.1007/s11214-012-9882-4>
- Maki, J. N., Golombek, M., Deen, R., Abarca, H., Sorice, C., Goodsall, T., et al. (2018). The color cameras on the InSight lander. *Space Science Reviews*, 214(6), 105. <https://doi.org/10.1007/s11214-018-0536-z>
- Maki, J. N., Lorre, J. J., Smith, P. H., Brandt, R. D., & Steinwand, D. J. (1999). The color of Mars: Spectrophotometric measurements at the Pathfinder landing site. *Journal of Geophysical Research*, 104(E4), 8781–8794. <https://doi.org/10.1029/98JE01767>
- Malin, M. C., Ravine, M. A., Caplinger, M. A., Tony Ghaemi, F., Schaffner, J. A., Maki, J. N., et al. (2017). The Mars Science Laboratory (MSL) Mast cameras and Descent imager: Investigation and instrument descriptions: MSL Mastcam/MARDI Descriptions. *Earth and Space Science*, 4(8), 506–539. <https://doi.org/10.1002/2016EA000252>
- Maxwell, J. C. (1860). On the theory of compound colours and the relations of the colours of the spectrum. *Proceedings of the Royal Society of London*, 10, 404–409. <https://doi.org/10.1098/rspa.1859.0074>
- Mutch, T. A., Binder, A. B., Huck, F. O., Levinthal, E. C., Liebes, S., Morris, E. C., et al. (1976). The surface of Mars: The view from the Viking 1 lander. *Science*, 193(4255), 791–801. <https://doi.org/10.1126/science.193.4255.791>
- Pascale, D. (2003). *A review of RGB color spaces... from xy to r'g'b'* (Vol. 18, pp. 136–152). The BabelColor Company. Retrieved from <https://babelcolor.com>
- Singer, R. B. (1982). Spectral evidence for the mineralogy of high-albedo soils and dust on Mars. *Journal of Geophysical Research*, 87(B12), 10159–10168. <https://doi.org/10.1029/JB087JB12p10159>
- Smith, P. H., Bell, J. F., Bridges, N. T., Britt, D. T., Gaddis, L., Greeley, R., et al. (1997a). Results from the Mars Pathfinder Camera. *Science*, 278(5344), 1758–1765. <https://doi.org/10.1126/science.278.5344.1758>
- Smith, P. H., Tomasko, M. G., Britt, D., Crowe, D. G., Reid, R., Keller, H. U., et al. (1997b). The imager for Mars Pathfinder experiment. *Journal of Geophysical Research*, 102(E2), 4003–4025. <https://doi.org/10.1029/96JE03568>
- Wyszecki, G., & Stiles, W. S. (1982). *Color science: Concepts and methods, quantitative data and formulae* (2nd ed.). New York: John Wiley.